

On the global character of overlap between low and high clouds

Tianle Yuan^{1,2} and Lazaros Oreopoulos¹

Received 17 July 2013; revised 9 August 2013; accepted 12 August 2013; published 1 October 2013.

[1] The global character of overlap between low and high clouds is examined using active satellite sensors. Low-cloud fraction has a strong land-ocean contrast with oceanic values double those over land. Major low-cloud regimes include not only the eastern ocean boundary stratocumulus and shallow cumulus but also those associated with cold air outbreaks downwind of wintertime continents and land stratus over particular geographic areas. Globally, about 30% of low clouds are overlapped by high clouds. The overlap rate exhibits strong spatial variability ranging from higher than 90% in the tropics to less than 5% in subsidence areas and is anticorrelated with subsidence rate and low-cloud fraction. The zonal mean of vertical separation between cloud layers is never smaller than 5 km and its zonal variation closely follows that of tropopause height, implying a tight connection with tropopause dynamics. Possible impacts of cloud overlap on low clouds are discussed. **Citation:** Yuan, T., and L. Oreopoulos (2013), On the global character of overlap between low and high clouds, *Geophys. Res. Lett.*, 40, 5320–5326, doi:10.1002/grl.50871.

1. Introduction

[2] Thin high clouds and low boundary layer clouds are two important cloud types in terms of cloud radiative effect. Thin high clouds are ubiquitous in the atmosphere [Liou 1986; Sassen *et al.*, 2008]. They trap outgoing longwave radiation and exert a net warming effect since they have only a minor influence on the shortwave radiation. Low boundary layer clouds on the other hand strongly modulate shortwave albedo while only weakly changing the longwave radiation. They are the primary contributor to the net climate cooling effect [Hartmann *et al.*, 1992]. Analysis of International Satellite Cloud Climatology Project data reveals that these vertically well-separated cloud types often coexist in the same geographic area, and this is corroborated by observations from other sources [Jakob and Tselioudis, 2003; Mace *et al.*, 2007]. In this type of high-over-low-cloud overlap, the net radiative impact of the two cloud types is expected to cancel out at the top of atmosphere to some degree. Furthermore, the presence of high clouds can significantly modify low-cloud top cooling/heating, primarily through their longwave effects, which can strongly affect low-cloud development [Chen and Cotton, 1987; Christensen *et al.*, 2013].

¹Climate and Radiation Laboratory, NASA Goddard Space Flight Center, Greenbelt, Maryland, USA.

²Joint Center for Environmental Technology and Department of Physics, UMBC, Baltimore, Maryland, USA.

Corresponding author: T. Yuan, Climate and Radiation Laboratory, NASA GSFC, Bldg. 33, Rm. A306, Mail Code 613, Greenbelt, MD 20771, USA. (tianle.yuan@nasa.gov)

[3] Before the advent of spaceborne active (lidar/radar) sensors, this type of overlap posed a challenge for passive sensors with regard to detecting the occurrence and characterizing the properties of the two cloud layers. Pure infrared (IR) techniques often misidentify the overlapping clouds as moderately thick midlevel clouds [Chang and Li, 2005a]. The CO₂-slicing technique provides a good detection method for identifying isolated high clouds, but in overlap situations can misidentify the two overlapped layers as a single thick high cloud. While a combined usage of CO₂-slicing, short-wave near IR and thermal IR channels can offer much better performances [Baum *et al.*, 1995; Pavolonis and Heidinger, 2004; Chang and Li, 2005a; Wind *et al.*, 2010] to unambiguously detect and better characterize overlapping clouds, active sensors are a much better option as demonstrated by studies of general statistics overlap and cloud vertical structure using such sensors [Wang and Dessler, 2006; Mace *et al.*, 2007].

[4] Previous works have shown that high-low cloud overlap type is quite prevalent throughout the globe [Warren *et al.*, 1985; Tian and Curry, 1989]. According to a study employing a two-layer retrieval technique on Moderate Resolution Imaging Spectroradiometer (MODIS) data [Chang and Li, 2005b], low clouds are overlapped by thin high clouds at a rate of 43% over land and 36% over ocean. Another survey with spaceborne lidar data shows that this type of overlap is the most frequent overlap type and about 32% of all tropical low clouds are overlapped by high cloud above [Wang and Dessler, 2006].

[5] Investigations on the origin of high-over-low-cloud overlap, its dynamic control and large-scale variations have been lacking. Here we use data from CloudSat and Cloud-Aerosol Lidar and Infrared Pathfinder Satellite Observations (CALIPSO) in conjunction with NASA Modern Era Retrospective-Analysis for Research and Applications (MERRA) [Rienecker *et al.*, 2011] reanalysis data to shed more light on certain aspects of this overlap.

2. Data and Method

[6] The CloudSat cloud profiling radar (CPR) is a 94 GHz nadir-looking radar, which records reflectivity from hydrometeors at effectively 250 m vertical and 1.5 km along-track resolutions [Marchand *et al.*, 2008]. It has a sensitivity of about −30 dBZ and can penetrate most cloud layers except those that are heavily precipitating. The Cloud-Aerosol Lidar with Orthogonal Polarization (CALIOP) is aboard CALIPSO which is part of the A-Train constellation along with CloudSat. CALIOP is a two-wavelength polarization-sensitive lidar that measures cloud and aerosols at a 333 m horizontal and 30–60 m vertical resolutions with a maximum penetration optical depth of about 3. Two different data sets are employed in this study. The main data set is the CloudSat-CALIPSO combined 2B-GEOPROF-Lidar product [Mace *et al.*, 2009]. The other is the CALIOP 1 km cloud layer product that reports

the occurrence of cloud layers using only the lidar signal [Vaughan *et al.*, 2004]. The CALIOP only product will likely miss overlaps when high clouds are sufficiently thick, while CloudSat CPR can penetrate moderately thick clouds and still detect low clouds above 1 km [Marchand *et al.*, 2008]. The combined product therefore represents the best spaceborne data source for our purposes despite occasional underestimates of low-cloud fraction by the CPR [Mace *et al.*, 2007; Mace *et al.*, 2009].

[7] Low clouds are defined here as having tops up to 3.5 km above the local topography or sea level, which is similar to the threshold of 680 hPa in previous studies [Rossow and Schiffer, 1999] except over highlands. The high clouds in this study are defined as having cloud base higher than 5 km relative to the local topography or higher than 7 km above sea level. When trying different thresholds to define low- and high-cloud layers, we find little sensitivity to threshold choice probably due to the well-known minimum of midlevel cloud occurrence [Zuidema, 1998; Chang and Li, 2005b].

[8] Low clouds occur throughout the tropics, subtropics, and midlatitudes. We set our study region between 60°S and 60°N to include different low-cloud regimes. We first search for low-cloud presence in the lidar/radar column and if a low cloud is found, a search for high clouds is conducted in the same column. From these profile-by-profile scans, the occurrence of nonoverlapped low clouds, high-over-low clouds, and all other situations can be aggregated in 2.5° grid cells. Along with the total number of observations, statistics such as monthly gridded total cloud fraction, low-cloud fraction, and overlap rate are calculated. The NASA MERRA reanalysis data are resampled to the same spatial grid to provide dynamic and thermodynamic context. We analyze data from January, April, July, and October of 2009 for both the CALIPSO 1 km cloud layer and the 2B-GEOPROF-LIDAR products, in order to characterize the full seasonal cycle. Unfortunately, due to the sun-synchronous orbits of the CALIPSO and CloudSat satellites, the diurnal characteristics of our cloud and overlap statistics cannot be resolved.

3. Results and Discussion

3.1. Low-Cloud Cover and Its Regimes

[9] The analysis of the 2B-GEOPROF-LIDAR product reveals that low clouds prefer ocean over land. Mean low-cloud fraction in oceanic grid cells, defined to be at least 80% covered by water, is 44% while it is 23% over land (all other grid cells). Land low-cloud fraction exceeds 40% over only two areas (Figure 1e), one in northern Europe surrounding the Baltic Sea and the other in the vicinity of southeast China. Values over northeastern Canada are also close to 40%. The common dynamic and thermodynamic conditions in these areas include a stable lower troposphere, moderate large-scale subsidence, and plentiful moisture flux from adjacent water surfaces as indicated by MERRA data (not shown here). While previous work has identified Southeast China as a region where semi-permanent stratus clouds are prevalent [Klein and Hartmann, 1993] (Figure 1a), North Europe and Northeast Canada have not been identified as such regions. Given that typical cloud fraction of low-level cumulus is less than 30% [Medeiros *et al.*, 2010], dominant cloud types over North Europe (Figure 1b) and Northeast Canada are likely stratus or fog.

[10] Almost everywhere, low-cloud fraction over other land areas is less than 30%, which suggests either a regime

change from stratus to fair-weather cumulus or more obscuration occurrences. Unobscured marine low-cloud fraction reaches minima throughout the deep tropics and maxima in major stratocumulus dominated areas (e.g., Figure 1c) and midlatitude storm track regions. Peak cloud fraction ranges from 80% in January and April to close to 100% in October and July and occurs exclusively in the eastern ocean boundary stratocumulus regime. Cloud fractions in trade cumulus dominated regions are much lower by comparison. Less attention has been paid to a regime of low clouds associated with cold air outbreaks in the winter season downwind of major continents [Atkinson and Zhang, 1996] (Figure 1d). These are formed when strong winds associated with cold air mass pick up moisture and heat from warm oceanic currents, creating favorable conditions for low-cloud formation [Young and Kristovich, 2002]. These clouds appear as “streets” with embedded closed cell stratocumulus (Figure 1d) and are responsible for local wintertime cloud fraction maxima east of the coasts of China, Japan, East Siberia, and North America (Figure 1d). This cloud regime does not appear as often in the part of the southern hemisphere, mostly because of the absence of the strong land-ocean temperature contrast encountered at northern midlatitudes.

3.2. High-Over-Low-Cloud Overlap

[11] The global-mean overlap rate, defined as the ratio of the number of profiles with overlap to the number of low-cloud profiles, is 30% in January 2009, with slightly higher values over land (32.6%) than over ocean (28.5%). However, it exhibits large spatial variations that are associated with clearly identifiable regimes. Maxima are reached in the tropical convective areas, in particular the Pacific Warm Pool and surrounding maritime continents where overlap rates of 80% are common. Over these areas, low clouds can only be detected in-between convective events. Due to the ubiquitous presence of cirrus clouds from either large-scale ascent or from dissipating deep convection, it is highly likely that a detected low cloud will be found overlapped by cirrus although overall low-cloud fraction is low in these areas (Figure 1). Minima are generally found over some land areas and over major stratocumulus dominated oceanic areas, where values can drop below 5%. These are regions of persistent strong subsidence, generally unfavorable for upper-level cloud formation. However, we note that even within this regime there are substantial seasonal and spatial variations and off the coast of California, it can reach up to 15–25%. The source of high cloud in these areas is mainly topography-driven gravity wave activity, advection from neighboring tropical convection centers such as Amazon Basin, Congo Basin, or ascent associated with midlatitude fronts. Intermediate values range from 35% to 65% in the midlatitude storm track regions in accordance with recent findings of thin cirrus prevalence in cyclonic systems [Posselt *et al.*, 2008; Sassen *et al.*, 2008; Naud *et al.*, 2012]. These three clearly defined regimes collectively result in a zonal mean pattern having one major peak in the tropics, two minor peaks in the midlatitudes, and two local minima in the subtropics (Figure 2b). The seasonal shift of the tropical convection manifests itself as a zonal shift in overlap rate maxima with the peak value staying about the same throughout this cycle. On the contrary, the magnitude of subtropical minima undergoes much more substantial seasonal changes, which warrants further investigation. Finally, we note a curious springtime strong local maximum

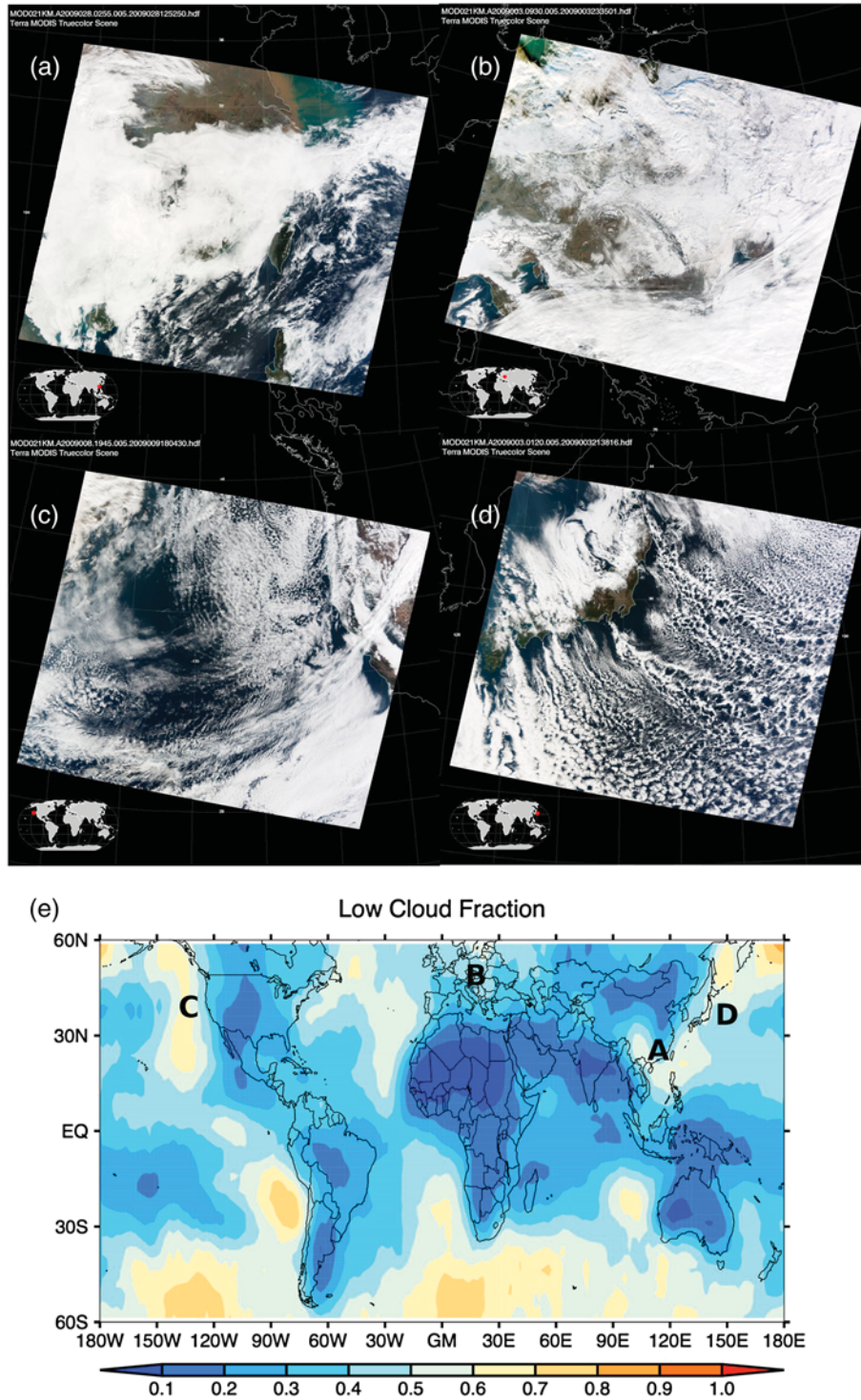


Figure 1. (a–d) Four representative cloud types as captured in January 2009 MODIS visible images, namely southeastern China stratus, northeastern Europe stratus, California stratocumulus, and roll/stratocumulus associated with cold air outbreaks downwind of Japan’s coast, respectively. (e) Total low-cloud fraction distribution for January of 2009 using combined CloudSat-CALIPSO cloud mask. The locations of Figures 1a–1d are marked on the map.

in the northern midlatitudes that may be a result of high-level dust transport being misidentified as high ice clouds or a manifestation of actual influences of dust on ice nucleation [Yu *et al.*, 2012].

[12] If we define the overlap rate as the ratio of the number of profiles with overlap to the total number of observations, the global-mean overlap rate is 12% with little seasonal

change, similar to what is reported in *Christensen et al.* [2013]. Given a total cloud fraction of ~60–70%, this particular type of cloud overlap occurs then about 17–20% of the time of cloudy occurrences. Its zonal structure shown in Figure 2c is qualitatively similar to that of Figure 2b, although the absolute maxima now switches between tropics and midlatitudes depending on the season. We note however

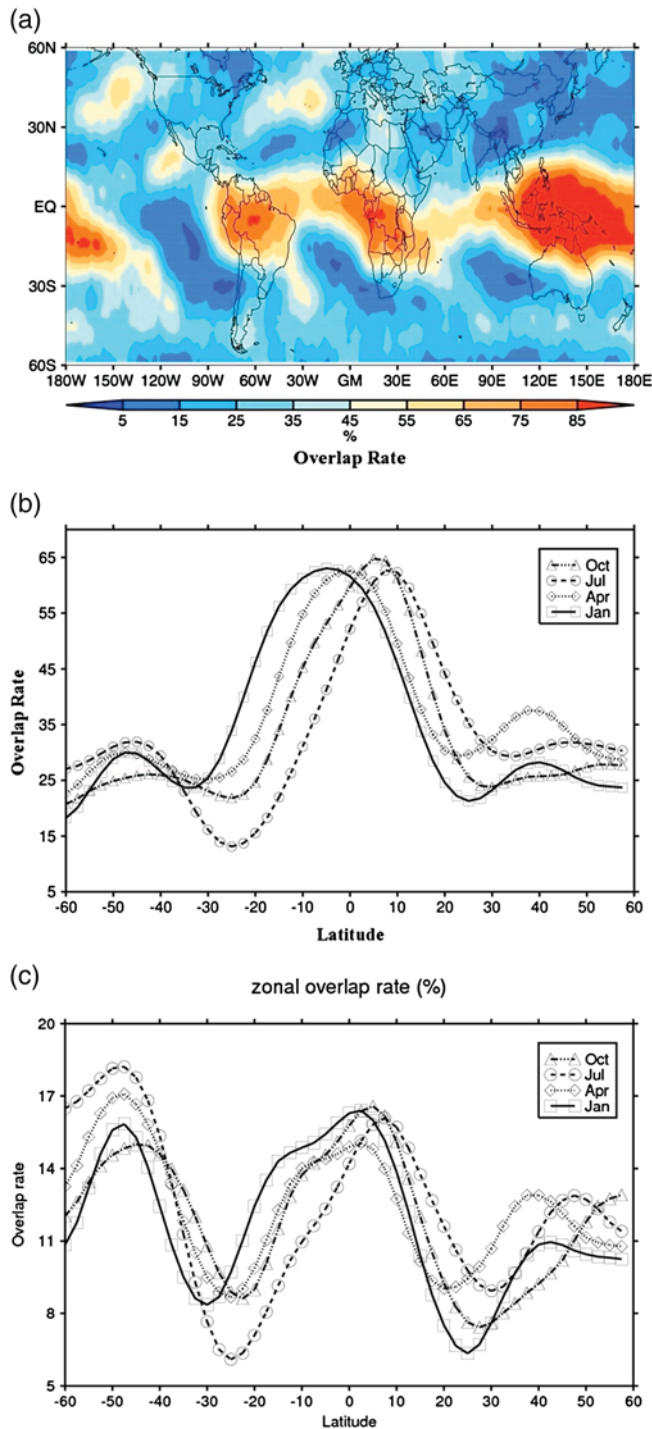


Figure 2. (a) Map of overlap rate for January 2009 from combined CloudSat-CALIPSO (2B-GEOPROF-LIDAR) data; (b) zonal mean overlap rate for 4 months representing different seasons using the same data set; and (c) similar to previous panel, but with the overlap rate defined as the ratio of the number of overlapped profiles to the total number of observed profiles.

that with this definition, the underestimation of overlap rate may be strongest in the tropics because thicker upper-level clouds, which pose problems for low-cloud detection by both sensors, are much more abundant [Mace *et al.*, 2009].

3.3. Dynamic Control

[13] As noted in the previous discussion, the overlap rate has clear regime dependence. Within the deep tropics, constant production and widespread occurrence of high clouds makes

high-over-low-cloud overlap highly likely whenever a low cloud is present. Gentle large-scale ascent and ice-cloud production from frontal convection are likely responsible for the local maximum in the midlatitude storm tracks. The strong and deep subsidence layer over the subtropical stratocumulus regions suppresses local production of ice clouds and reduces the overlap to a minimum. Here we use MERRA monthly pressure vertical velocity data at 500 hPa (Ω_{500}) and 700 hPa (Ω_{700}) as a proxy for dynamic regimes and

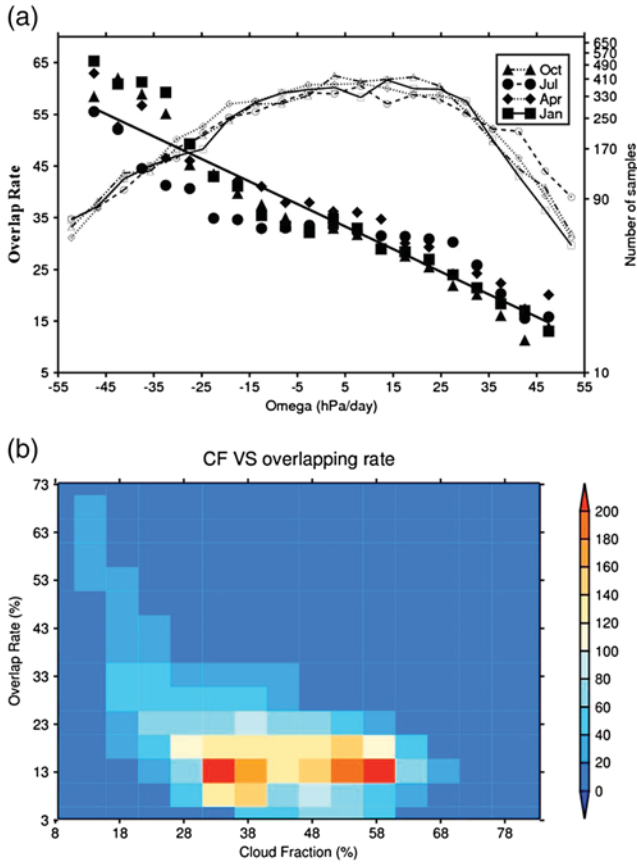


Figure 3. (a) Relationship between Omega at 700 mb and overlap rate for January, April, July, and October of 2009. Filled symbols are actual data while unfilled symbols represent the number of samples. (b) Relationship between overlap rate and low-cloud fraction.

investigate the relationship between the overlap rate and the dynamic condition.

[14] We find good anticorrelation between Omega700 (or Omega500) and the monthly gridded overlap rate (correlation coefficient $r = -0.94$, and probability of the null hypothesis $p < 0.001$) over the ocean. The frequency distribution of Omega700 is negatively skewed; and to include sufficient samples for each bin, we limit our calculation within the range of -50 to 50 hPa/day. Overlap rate data are averaged within 5 hPa/day bins. The overlap rate increases with decreasing Omega700 at a rate of about $0.45\%/hPa$, and the intercept with zero vertical velocity is around 35%. Scaling is found for all months examined with similar slope and intercept. A similar relationship is found if Omega500 is used and is therefore not shown here. Qualitatively, the correlation is expected because of the clearly defined cloud system regimes and the vertical velocity associated with them. However, existence of such a robust quantitative scaling is not trivial. The slope and intercept of this linear relationship are not sensitive to seasonal changes, which makes it a useful constraint for diagnosing model performances of this type of overlap occurrence. When the alternate overlap rate definition of Figure 2c is used, a similar anticorrelation with Omega700 and Omega500 is found (results not shown here).

[15] An anticorrelation ($r = -0.56$, $p < 0.001$) exists between low-cloud fraction and overlap rate over the ocean (Figure 3b). This is easily understood because the strong subsidence favors

low-cloud formation and suppresses ice-cloud generation. However, the fact that these two cloud types can still coexist under this condition makes this type of overlap challenging and interesting to represent in models. Topographically and convectively generated gravity waves are likely candidates for generating high clouds in these large-scale subsidence regions.

3.4. Vertical Separation

[16] Our definitions require that high clouds have bases either 5 km above local topography or 7 km above sea level and that the top of low clouds is below 3.5 km above the local topography or sea level. These definitions of high and low clouds do not in principle restrict their vertical separation to large values. Our data set indicates (Figure 4a) that the vertical separation between the two cloud layers has a clear zonal dependence, but is never smaller than 5 km in the zonal mean, highlighting the absence of midlevel clouds and the well-separated nature of these cloud types. The height difference reaches maximum in the tropics while it falls to a minimum over highland areas such as the Himalayas, the Iranian Plateau, and the Rocky Mountains. These minima are due in a large part to the high-ground elevation. Since low-cloud top heights do not exhibit systematic zonal variations (figure not shown), most of the zonal structure in vertical separation comes

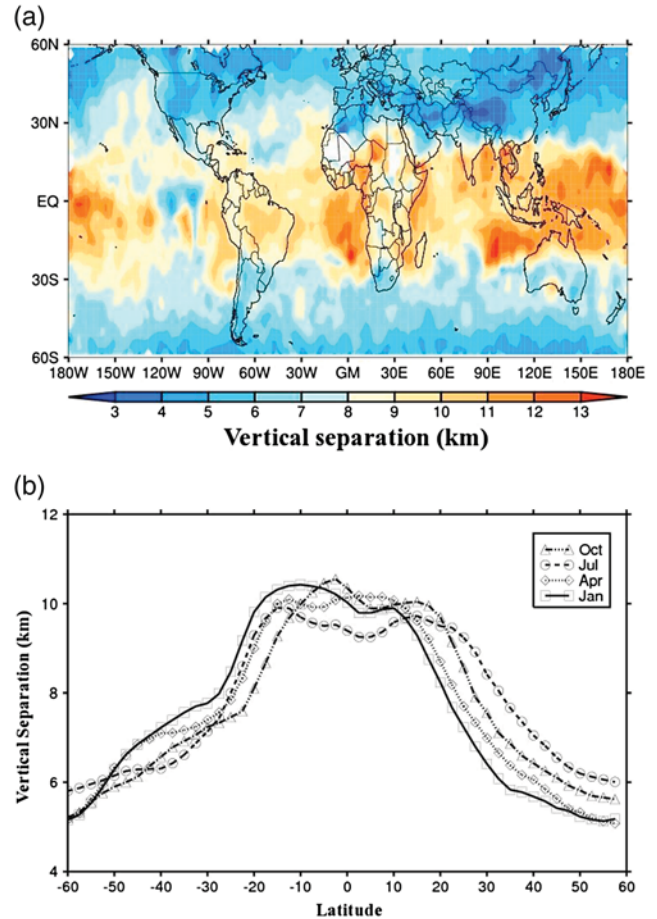


Figure 4. (a) The separation distance between the base of high cloud and the top of the low cloud when overlap occurs in January 2009; (b) zonal mean vertical separation between high and low clouds for the four 2009 months we use to represent different seasons.

from zonal variations of high-cloud altitude which should be closely related to the thermodynamic structure of the upper atmosphere. In fact, the strong latitudinal dependence of the height difference (Figure 4b) follows closely the zonal structure of tropopause height [Schmidt *et al.*, 2010]. The vertical separation decreases from 11 km in the tropics to around 5 km at higher latitudes. The 6 km difference is similar to the tropopause height variations between the tropics and high latitudes ($\sim 60^{\circ}\text{S}$ and $^{\circ}\text{N}$), and the overall zonal structures of these two are quite similar [Schmidt *et al.*, 2010]. There is also a clear seasonal cycle in the magnitude of vertical separation between two cloud layers. This seasonal cycle is stronger in the Northern Hemisphere than that in the Southern Hemisphere, similar to the seasonal cycle of tropopause height [Schmidt *et al.*, 2010; Li *et al.*, A global survey of the linkages between cloud vertical structure and large-scale climate, submitted to *Journal of Geophysical Research Atmosphere*, 2013]. We therefore believe that only few midlevel clouds overlap with low clouds, and the variations in height of upper-level clouds are strongly tied to tropopause dynamics.

3.5. Discussion

[17] The well-separated nature of the overlap makes feasible the application of dual cloud layer retrievals with passive sensors [Chang and Li, 2005b; Minnis *et al.*, 2007]. It also points to the potential radiative impact of this cloud overlap, especially in the longwave when high cloud is thin. It is expected that the radiative interactions between the two cloud layers will have implications for the evolution of both cloud types, but especially of low clouds. We plan to comprehensively assess these radiative interactions and their impact in a separate study. Our preliminary results suggest significant changes in both the mean and diurnal cycle of low-cloud properties such as cloud fraction, liquid water path, precipitation, and even organization [Chen and Cotton, 1987; Wang and Feingold, 2009; Christensen *et al.*, 2013] due to the presence of high clouds aloft.

4. Summary

[18] Active spaceborne sensors are used to study the specific case of overlap between high and low clouds. The low-cloud fraction distribution captured by the combined radar-lidar data agrees with previous work, but additional new insights are gained. Three distinct overlapping regimes are identified to be associated with tropical convection, midlatitude storms, and remote/local gravity wave generated high clouds over subsidence regions. The overlap rate decreases in that order, in accordance with our qualitative understanding of dynamics associated with each regime. Globally, 30% of low clouds are overlapped by high clouds aloft. This accounts for 12% of the total observations. Large-scale pressure vertical velocity is found to anti-correlate well with the overlap rate throughout the year. The high and low layers are well separated vertically with the zonal mean of the vertical separation being always greater than 5 km, exposing thus the scarcity of midlevel clouds. The zonal structure of the vertical separation between the two cloud layers and its seasonal cycle follows closely those of tropopause height, which may be indicative of high clouds being strongly coupled with tropopause dynamics.

[19] **Acknowledgments.** The authors acknowledge funding support from NASA's CALIPSO-CloudSat and Radiation Science programs. We also thank the reviewers for helpful comments and suggestions.

[20] The Editor thanks two anonymous reviewers for their assistance in evaluating this paper.

Reference

- Atkinson, B., and J. Zhang (1996), Mesoscale shallow convection in the atmosphere, *Rev. Geophys.*, *34*(4), 403–431.
- Baum, B. A., T. Uttal, M. Poellot, and T. P. Ackerman (1995), Satellite remote sensing of multiple cloud layers, *J. Atmos. Sci.*, *52*, 4210–4230.
- Chang, F. L., and Z. Li (2005a), A new method for detection of cirrus overlapping water clouds and determination of their optical properties, *J. Atmos. Sci.*, *62*, 3993–4009.
- Chang, F.-L., and Z. Li (2005b), A near-global climatology of single-layer and overlapped clouds and their optical properties retrieved from Terra/MODIS data using a new algorithm, *J. Clim.*, *18*(22), 4752–4771, doi:10.1175/JCLI3553.1.
- Chen, C., and W. R. Cotton (1987), The physics of the marine stratocumulus-capped mixed layer, *J. Atmos. Sci.*, *44*, 2951–2977, doi:10.1175/1520-0469(1987)044<2951:TPOTMS>2.0.CO;2.
- Christensen, M. W., G. Carrio, G. L. Stephens, and W. R. Cotton (2013), Radiative impacts of free-tropospheric clouds on the properties of marine stratocumulus, *J. Atmos. Sci.*, doi:10.1175/JAS-D-12-0287.1, in press.
- Hartmann, D. L., M. E. Ockertbell, and M. L. Michelsen (1992), The effect of cloud type on Earth's energy balance: Global analysis, *J. Clim.*, *5*(11), 1281–1304.
- Jakob, C., and G. Tselioudis (2003), Objective identification of cloud regimes in the Tropical Western Pacific, *Geophys Res Lett.*, *30*(21), 2082, doi:10.1029/2003GL018367.
- Klein, S. A., and D. L. Hartmann (1993), The seasonal cycle of low stratiform clouds, *J. Clim.*, *6*, 1587–1606, doi:10.1175/1520-0442(1993)006<1587:TSCOLS>2.0.CO;2.
- Liou, K. N. (1986), Influence of cirrus clouds on weather and climate processes: A global perspective, *Mon. Weather Rev.*, *114*, 1167–1199, doi:10.1175/1520-0493(1986)114<1167:IOCCOW>2.0.CO;2.
- Mace, G. G., R. Marchand, Q. Zhang, and G. Stephens (2007), Global hydrometeor occurrence as observed by CloudSat: Initial observations from summer 2006, *Geophys. Res. Lett.*, *34*, L09808, doi:10.1029/2006GL029017.
- Mace, G. G., Q. Zhang, M. Vaughan, R. Marchand, G. Stephens, C. Trepte, and D. Winker (2009), A description of hydrometeor layer occurrence statistics derived from the first year of merged Cloudsat and CALIPSO data, *J. Geophys. Res.*, *114*, D00A26, doi:10.1029/2007JD009755.
- Marchand, R., G. G. Mace, T. Ackerman, and G. L. Stephens (2008), Hydrometeor detection using CloudSat—An Earth-orbiting 94-GHz cloud radar, *J. Atmos. Oceanic Technol.*, *25*, 519–533, doi:10.1175/2007JTECHA1006.1.
- Medeiros, B., L. Nuijens, C. Antoniazzi, and B. Stevens (2010), Low-latitude boundary layer clouds as seen by CALIPSO, *J. Geophys. Res.*, *115*, D23207, doi:10.1029/2010JD014437.
- Minnis, P., J. Huang, B. Lin, Y. Yi, R. F. Arduini, T. Fan, J. K. Ayers, and G. G. Mace (2007), Ice cloud properties in ice-over-water cloud systems using Tropical Rainfall Measuring Mission (TRMM) visible and infrared scanner and TRMM microwave imager data, *J. Geophys. Res.*, *112*, D06206, doi:10.1029/2006JD007626.
- Naud, C. M., D. J. Posselt, and S. C. van den Heever (2012), Observational analysis of cloud and precipitation in mid-latitude cyclones: Northern versus Southern Hemisphere warm fronts, *J. Clim.*, *25*, 5134–5151.
- Pavolonis, M. J., and A. K. Heidinger (2004), Daytime cloud overlap detection from AVHRR and VIIRS, *J. Appl. Meteorol.*, *43*(5), 762–778, doi:10.1175/2099.1.
- Posselt, D. J., G. L. Stephens, and M. Miller (2008), CloudSat: Adding a new dimension to a classical view of extratropical cyclones, *Bull. Am. Meteorol. Soc.*, *89*, 599–609.
- Rienecker, M. M., et al. (2011), MERRA: NASA's Modern-Era Retrospective Analysis for Research and Applications, *J. Clim.*, *24*, 3624–3648, doi:10.1175/JCLI-D-11-00015.1.
- Rossov, W., and R. Schiffer (1999), Advances in understanding clouds from ISCCP, *Bull. Am. Meteorol. Soc.*, *80*(11), 2261–2287.
- Sassen, K., Z. Wang, and D. Liu (2008), Global distribution of cirrus clouds from CloudSat/Cloud-Aerosol lidar and infrared pathfinder satellite observations (CALIPSO) measurements, *J. Geophys. Res.*, *113*, D00A12, doi:10.1029/2008JD009972.
- Schmidt, T., J. Wickert, and A. Haser (2010), Variability of the upper troposphere and lower stratosphere observed with GPS radio occultation bending angles and temperatures, *Adv. Spa. Res.*, *46*, 150–161.
- Tian, L., and J. A. Curry (1989), Cloud overlap statistics, *J. Geophys. Res.*, *94*(D7), 9925, doi:10.1029/JD094iD07p09925.

- Vaughan, M. A., S. A. Young, D. M. Winker, K. A. Powell, A. H. Omar, Z. Liu, Y. Hu, and C. A. Hostetler (2004), Fully automated analysis of space-based lidar data: An overview of the CALIPSO retrieval algorithms and data products, *Remote Sens.*, 5575, 16–30, doi:10.1117/12.572024.
- Wang, H., and G. Feingold (2009), Modeling mesoscale cellular structures and drizzle in marine stratocumulus. Part I: Impact of drizzle on the formation and evolution of open cells, *J. Atmos. Sci.*, 66(11), 3237–3256, doi:10.1175/2009JAS3022.1.
- Wang, L., and A. E. Dessler (2006), Instantaneous cloud overlap statistics in the tropical area revealed by ICESat/GLAS data, *Geophys. Res. Lett.*, 33, L15804, doi:10.1029/2005GL024350.
- Warren, S. G., C. J. Hahn, and J. London (1985), Simultaneous occurrence of different cloud types, *J. Climate Appl. Meteorol.*, 24, 658–667.
- Wind, G., S. Platnick, M. D. King, P. A. Hubanks, M. J. Pavolonis, A. K. Heidinger, P. Yang, and B. A. Baum (2010), Multilayer cloud detection with the MODIS near-infrared water vapor absorption band, *J. Appl. Meteorol. And Climatol.*, 49(11), 2315–2333, doi:10.1175/2010JAMC2364.1.
- Young, G. S., and D. Kristovich (2002), Rolls, streets, waves, and more: A review of quasi-two-dimensional structures in the atmospheric boundary layer, *Bull. Am. Meteorol. Soc.*, 83, 997–1001.
- Yu, H., L. A. Remer, M. Chin, H. Bian, Q. Tan, T. Yuan, and Y. Zhang (2012), Aerosols from overseas rival domestic emissions over North America, *Science*, 337(6094), 566–569, doi:10.1126/science.1217576.
- Zuidema, P. (1998), The 600–800-mb minimum in tropical cloudiness observed during TOGA COARE, *J. Atmos. Sci.*, 55, 2220–2228.